Thin Solid Films 398–399 (2001) 413–418

www.elsevier.com/locate/tsf

Structures and properties of the SiNC films on Si wafer at different deposition stages

Jin-Yu Wu, Cheng-Tzu Kuo*, Tzu-Lung Liu

Department of Materials Science and Engineering, National Chiao Tung University, 1001 Ta-Hsueh Road, Hsinchu 300, Taiwan, ROC

Abstract

The films were deposited on Si wafer by a microwave plasma chemical vapor deposition (MPCVD) system with CH_4, N_2, up to 8.3 vol.% H_2 and additional Si chips as the sources. The films were examined at different deposition times to explore different growth stages of deposition. Examination indicated the deposition can be roughly divided up to three stages, depending on deposition time and based on their structure and property. In the early deposition stages, the films consist of two layers, i.e. Si-oxide and SiNC layers. The SiNC layer consists essentially of nano-crystals embedded in ternary SiNC amorphous matrix with crystal structure close to SiC. In contrast, in the later stage, the films are further covered by a layer of the binary SiN crystalline phases with crystal structures much closer to α-Si_3N_4 than β-Si_3N_4 and tetragonal Si_3N_4 type structures. The band gaps, as revealed by CL (cathodoluminescence) spectra, are $\sim$3.88 eV (320 nm) for SiN layer and $\sim$2.82 eV (440 nm) for SiNC layer. Depending on the deposition conditions, the growth competitions among SiC, Si–N and SiNC crystalline phases may result in different morphologies, compositions and properties of the films. © 2001 Elsevier Science B.V. All rights reserved.

Keywords: Silicon carbon nitride; Deposition mechanism; MPCVD; Nano-indentation

1. Introduction

Recently, syntheses of new materials for field emission and/or wear resistant applications have attracted much attention [1–4]. The candidate materials include diamond, CN and SiNC, which are proved either theoretically or experimentally to be the materials possessing excellent field emission properties and super hardness [5–9]. Many methods have been developed to synthesize SiNC films, for example microwave plasma chemical vapor deposition (MPCVD) [10–13], magnetron sputtering [14], dual ion gun [15], pulse laser deposition (PLD) [16–18] and hot filament chemical vapor deposition (HFCVD) [18,19]. Most of the researchers claimed that the deposited films are either ternary SiNC amorphous or silicon carbon nitride crystalline phases. These investigators used the results of ESCA or AES to prove the existence of ternary SiNC films, and the results of XRD or electron diffraction (ED) as the evidence of crystalline films. However, the reported results are either ambiguous or contradictory. The motivation of this work was to study the deposition mechanisms by examining the progress of deposition, composition and property variations at different deposition times, and to clarify the growth competitions among various binary and ternary phases.

2. Experimental

The films were deposited on Si wafers by a MPCVD system with CH_4, N_2, 0.0–8.3 vol.% H_2 as raw sources. The Si columns inserted in a specimen holder around the symmetrical positions of Si substrate were used as the additional Si source. Some of the substrates were subjected to Si_3N_4 powder scratching in acetone solution to act as seeding pretreatment before film deposition. The deposition conditions were as follows: flow ratio of $CH_4/N_2 = 10{:}100$ sccm/sccm; of $H_2/N_2 =$ either 0:100 or 10:100 sccm/sccm; microwave power 950 W; total pressure 2×10^3 Pa; substrate temperatures 1100–1200°C

* Corresponding author. Tel.: +886-3-5714212; fax: +886-3-5724727.

E-mail address: ctkuo@cc.nctu.edu.tw (C.-T. Kuo).

0040-6090/01/$ - see front matter © 2001 Elsevier Science B.V. All rights reserved.
PII: S0040-6090(01)01350-5

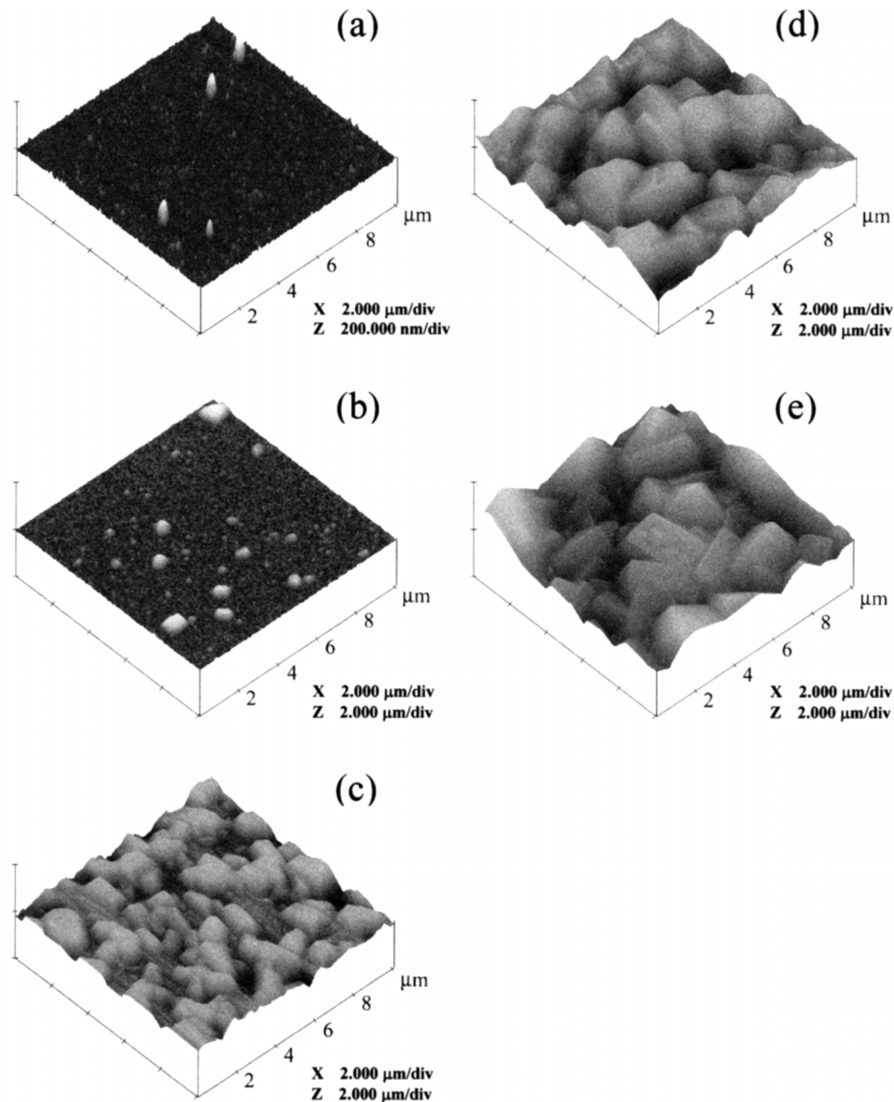

Fig. 1. Typical AFM micrographs of the film surfaces at different deposition times: (a) 1/3 h, (b) 1/2 h, (c) 1 h, (d) 2 h, (e) 5 h.

and deposition time 0.3–6 h. A Hysitron nano-indentation system and *I–V* meters were used to determine the mechanical and field emission properties.

3. Results and discussion

3.1. Film morphologies and structures at different deposition times

The typical AFM morphologies of the SiNC films at different deposition times of 1/3, 1/2, 1, 2 and 5 h are shown in Fig. 1. In the earlier deposition stages (<1 h, Fig. 1a,b), the film surfaces reveal a few crystallites embedded in a smooth film of nano-sized roughness. The crystallites are less than 300 nm in diameter. It signifies that the smooth film is formed on the substrate surface before crystallite nucleation and growth. In the later deposition stages with 1, 2 and 5 h of deposition times (Fig. 1c–e), the faceted crystals entirely cover the original smooth film surfaces. The faceted crystals reveal hexagonal morphologies.

The crystal structures of the films at different deposition times were also examined by XRD, as depicted in Fig. 2a,b, where Fig. 2b is for films deposited by adding 8.3 vol.% H_2 in the source gases. These figures indicate that the films in the earlier deposition stages are almost amorphous in structure without significant diffraction peaks in the XRD patterns. In the later stages, the diffraction peaks appear first at planes of α-Si_3N_4 (210), β-Si_3N_4 (100), and tetragonal-Si_3N_4 (220), and then become more diffraction planes at higher deposition times. It implies that the films consist of a mixture of different crystalline phases at higher deposition times. As to the effect of adding 8.3 vol.% H_2 in Fig. 2b, it appears that the peak positions are almost same as in Fig. 2a, except the relative peak intensities are different.

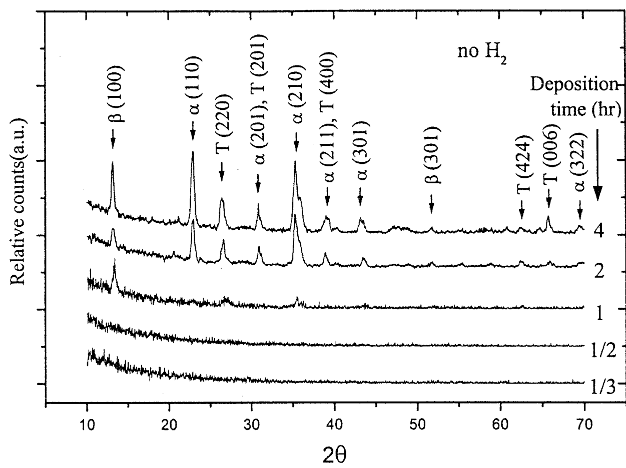

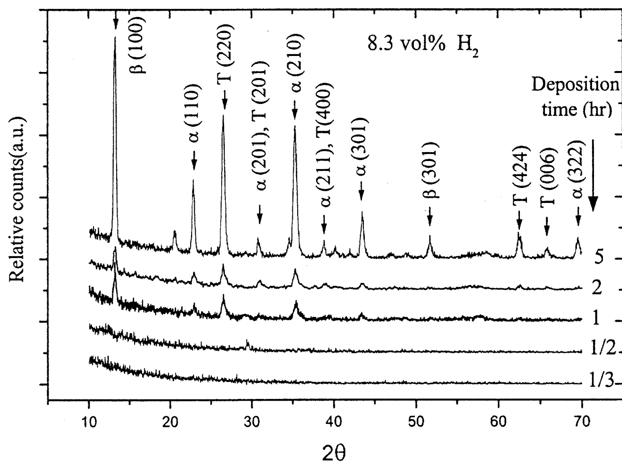

Fig. 2. Typical XRD patterns of the film surfaces at different deposition times: (a) without H_2 and (b) with 8.3 vol.% H_2 in the source gases.

The film cross-sections at higher deposition times were studied by TEM and electron diffraction (ED) analyses. Fig. 3a–d depict the TEM micrographs of the film cross-section and the corresponding selected area ED patterns. Fig. 3b is a magnified micrograph of Fig. 3a, and can be divided into three layers except Si substrate. Fig. 3c is a ED pattern with beam in the ⟨001⟩ zone axis, which represents a hexagonal structure for the top crystalline layer. The ED pattern in Fig. 3d is a polycrystalline ring pattern for the second layer, which is similar to diamond-like carbon structure with nano-sized crystallites embedded in an amorphous matrix. The detailed comparisons of Fig. 3d with various phases of Si_3N_4 and SiC structures are shown in Table 1. It indicates that the structures of the second layer match well with SiC structures instead of Si_3N_4 structures. As will be discussed in the next paragraphs, the top, the second and the third layers essentially consist of binary Si–N crystals, ternary SiNC polycrystalline phases in amorphous matrix, and Si oxides, respectively.

The bonding structures of the Si substrate and the films with two different deposition times (1/3 h and 6 h) are depicted by the FTIR spectra in Fig. 4. There are Si–C and Si–O bonds for films of 1/3-h deposition time, which correspond to the bonding of the second and third layers in Fig. 3b. However, there are mainly Si–N bonds for films of 6-h deposition time, which corresponds to the bonding of the top layer. The results are in agreement with the morphology examination in Fig. 1 and the crystal structure analyses in Figs. 2 and 3.

3.2. Film compositions

The TEM+EDS selected area composition analyses for the second layer in Fig. 3b were conducted, which represent the compositions of the films of lower deposition times, such as shown in Fig. 1a. The films at the earlier deposition stages essentially consist of a mixture of ternary SiNC phases in amorphous matrix (64.0–68.3 at.% Si+9.0–16.3 at.% N+9.7–22.8 at.% C). The same composition analyses reveal that the crystals of the top and the third layers are mainly binary Si–N crystalline phases (atomic ratio of Si/N=1.9–3.9) and Si-oxides, respectively. The thickness is approximately ∼200 nm

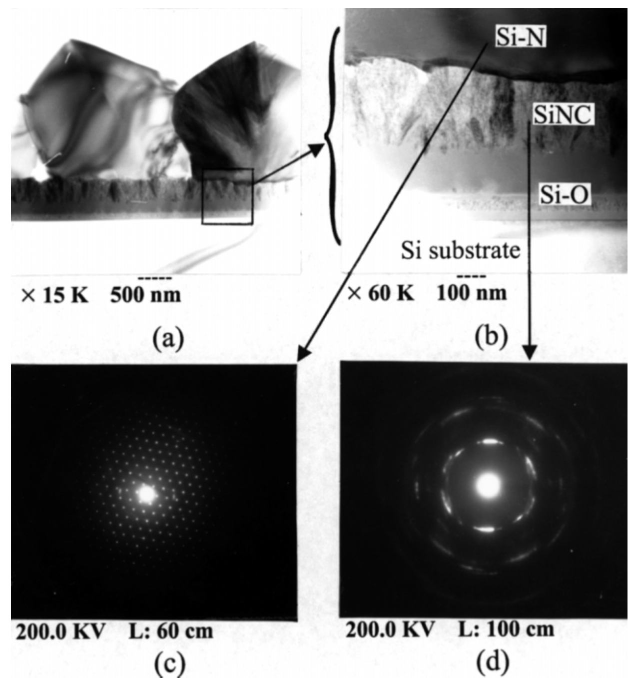

Fig. 3. Typical TEM micrographs and ED patterns of the cross-sections of the films at 6-h deposition time: (a) 15 k, (b) 60 k magnifications, (c) the selected area ED patterns with ⟨001⟩ zone axis, (d) the selected area ED pattern, as indicated in (b).

for the second SiNC layer, which is not sensitive to the variation of deposition time; and is approximately ~2 μm for the top Si–N crystalline layer at 6-h deposition time.

The typical ESCA depth profile analyses for the film of 5-h deposition time is depicted in Fig. 5. The results show that the compositions starting from the free surface are high O–C layers and then high Si–N layers. It appears to be in disagreement with the results of the previous paragraphs, where the top layer is proved to be the Si–N layer. This can be reasoned by the facts that the O–C layer could be deposited during the cooling stage after film deposition, or come from the contamination from the air atmosphere. The O–C layer is so loosely adhered on the film surface, and can be readily mixed with the bonding materials for TEM sample preparation. Therefore, the O–C layer could not be seen in the TEM micrographs in Fig. 3. Fig. 5 also shows that the Si/N ratios at higher sputtering times are approximately ~1.44, which are the same order of magnitude to the values analyzed by EDS.

3.3. Seeding effect by Si_3N_4 powder scratching

The previous analyses indicate that the deposited films at the deposition time greater than 1 h is essentially covered by a binary Si–N layer. Therefore, the Si_3N_4 powder scratching on the substrate might enhance the Si–N nucleation. Fig. 6a,b compare the SEM morphologies of the films deposited on substrates without and with pretreatment of the Si_3N_4 powder scratching, respectively. It shows a two-order of magnitude improvement in nucleation density for film with the Si_3N_4 powder scratching. The nucleation densities in Fig. 6a,b are 0.08 and 5.5 μm^{-2}, respectively. The residues of Si_3N_4 powders appear to act as the effective seeds for nucleation of the top Si–N crystals. This signifies that under the present deposition conditions, no matter whether there is substrate scratching by Si_3N_4 powders or not, it is the more favored condition to grow binary silicon nitrides instead of ternary silicon carbon nitrides, except at the earlier deposition stages, as discussed in the previous paragraphs.

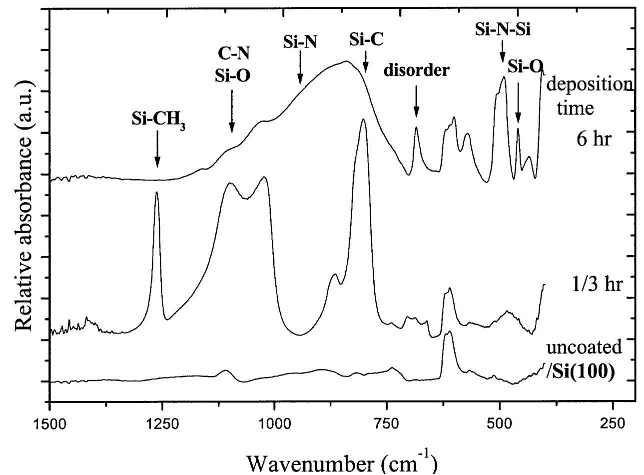

Fig. 4. FTIR spectra for Si wafer, the films with 1/3-h and 6-h deposition times.

3.4. Film properties

Effect of deposition time on the CL spectra of the films is shown in Fig. 7. It suggests that the CL peak

Table 1
Comparison of the calculated d_{hkl} spacings from ED analyses for SiNC layer with the values from the literature for various phases of Si_3N_4 and SiC crystals

hkl plane	Calculated *d*(*hkl*) (Å)	α-Si_3N_4 *d*(*hkl*) (Å)[a]	β-Si_3N_4 *d*(*hkl*) (Å)[a]	T–Si_3N_4 *d*(*hkl*) (Å)[a]	α-SiC *d*(*hkl*) (Å)[b]	SiC *d*(*hkl*) (Å)[c]	SiC *d*(*hkl*) (Å)[d]
100	2.72573	6.71	6.583		2.67	2.669	2.669
002	2.57275	2.811	1.4534	4.2835			2.515
101	2.40123	4.3098	2.660		2.59	2.579	2.357
102	1.88861	2.593	1.4197	3.8292	2.36	2.357	1.8304
110	1.60082	3.877	3.8	6.5795	1.54	1.5407	1.5407
103	1.45739	1.8046	0.9589		2.08	2.088	1.4198
200	1.35190	3.359	3.293	4.6829		1.3343	1.3343
201	1.30299	2.883	2.1797			1.3227	1.2897
202	1.22096	2.155	1.3299		1.29	1.2897	1.1787
203	1.06160		0.9298		1.24	1.2398	1.0441
210	1.02910	2.538	2.489				1.0087
212	0.96973	1.8837	1.2554		0.98	0.98	0.9362
213	0.87545	1.5068			0.96		0.8643
310	0.75942	1.8627	1.8275				
312	0.72037	1.5521	1.1377				

[a] From JCPDS cards: 41-0360: hexagonal α-Si_3N_4; 33-1160: hexagonal β-Si_3N_4; 40-1129: tetragonal T–Si_3N_4.
[b] From JCPDS cards: 02-1462: hexagonal α-SiC.
[c] From JCPDS cards: 29-1127: hexagonal SiC.
[d] From JCPDS cards: 29-1126: hexagonal SiC.

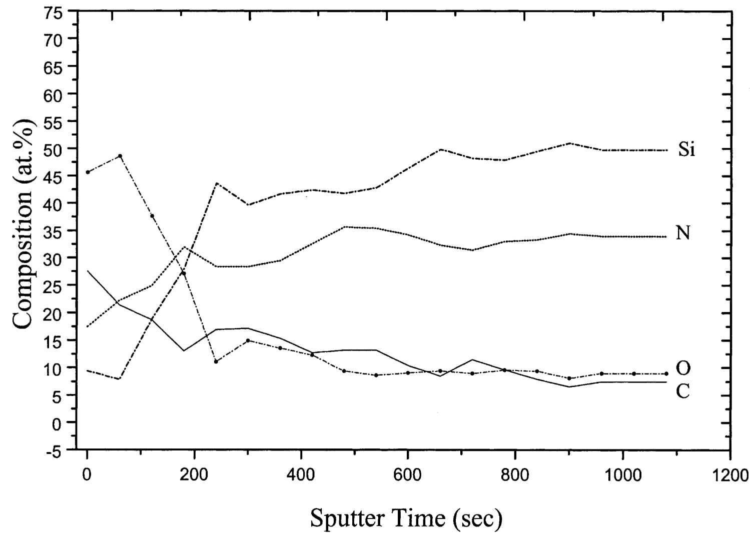

Fig. 5. Typical ESCA depth profile of the films.

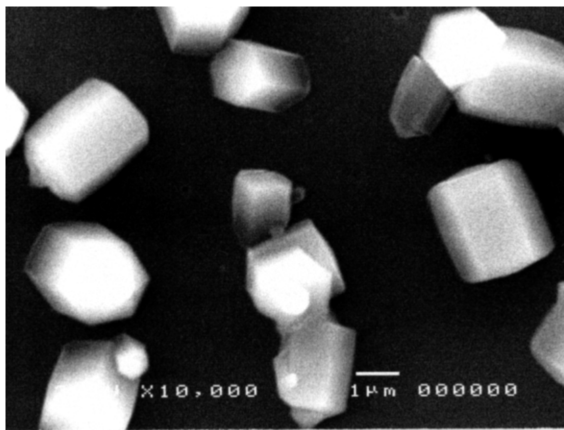

(a)

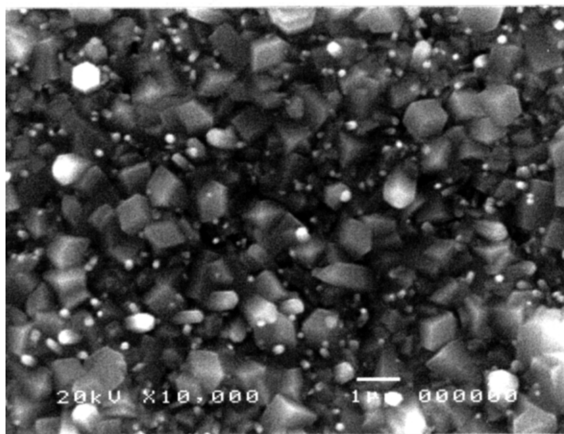

(b)

Fig. 6. SEM micrographs of the film surfaces: (a) substrate without scratching, (b) substrate scratching with Si_3N_4 powders before film deposition.

positions can be changed from ~440 nm at the earlier deposition stages to ~320 nm at the higher deposition times. As discussed in previous paragraphs, the peak positions of 440 nm (or 2.82 eV) and 320 nm (or 3.88 eV) may correspond to emission of the SiNC and the Si–N layers, respectively.

The selected area mechanical properties of the films were estimated by a Hysitron nano-indentation system. The nano-hardness and the reduced modulus of the Si–N crystalline layer of the films are approximately 26–33 and 271–381 GPa, respectively. In contrast, the corresponding values for the SiNC layer are approximately 15–22 and 151–201 GPa, respectively, which can include more substrate effects due to a much smaller film thickness.

The field emission properties of the films of 6-h deposition time were determined by *I–V* measurements,

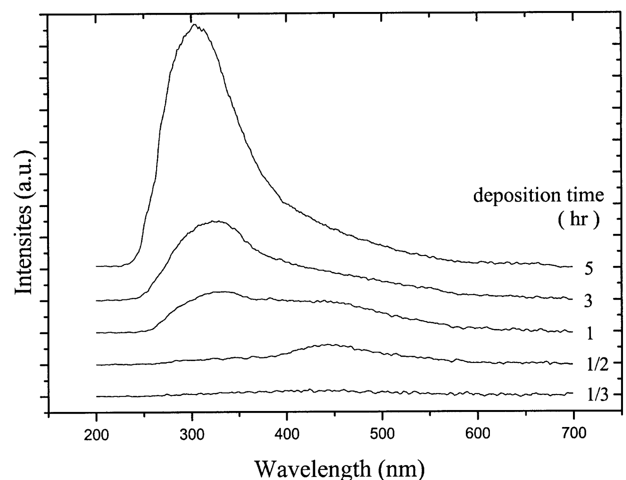

Fig. 7. CL spectra of the films at different deposition times.

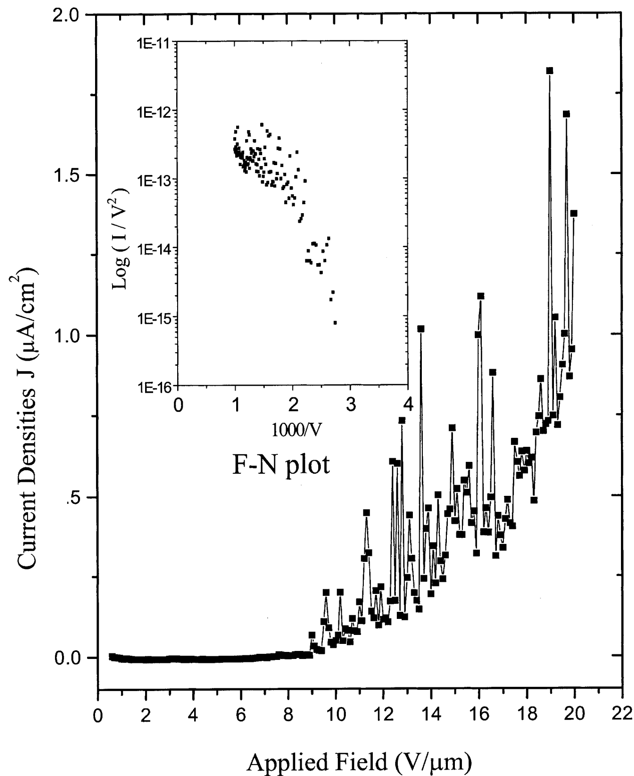

Fig. 8. The field emission properties of the film at 6-h deposition time.

as shown in Fig. 8. The turn-on-applied field can go as low as $\sim$9 V/μm. The current density at 20 V/μm can reach $\sim$6.3 $\mu A/cm^2$.

4. Conclusions

Based merely on the results of the film surface analyses, such as ESCA, XRD and SEM, it might often give a false impression of forming ternary silicon carbon nitride crystalline films, as reported in the literature. Under the present deposition conditions, the deposited films can be divided up to three distinct layers depending on deposition times, i.e. Si–O, SiNC and Si–N layers. The crystal structures of the SiNC layer consist of nano-sized crystallites embedded in amorphous matrix, where crystallites are close to the SiC crystal structure. In contrast, the crystal structures of the Si–N layer are a mixture of various Si_3N_4 phases. The results also imply that there are growth competitions among various Si–N, SiC and SiNC crystals. Under the present deposition conditions, the Si–N phases must be more favored phases after longer deposition times.

Acknowledgements

This work was supported by the National Science Council (contract no.: NSC89-2216-E-009-020 and-019) and the Ministry of Education of Taiwan (contract no.: 89-E-FA06-1-4).

References

[1] Q.A. Huang, M.C. Poon, J.K.O. Sin, Appl. Surf. Sci. 119 (3-4) (1997) 229–236.
[2] E.P. Sheshin, A.V. Anashchenko, S.G. Kuzmenko, Ultramicroscopy 79 (1-4) (1999) 109–114.
[3] P.W. May, M.T. Kuo, M.N.R. Ashfold, Diam. Relat. Mater. 8 (1999) 1490–1495.
[4] M.T. Kuo, P.W. May, A. Gunn, J.C. Marshall, M.N.R. Ashfold, K.N. Rosser, Int. J. Mod. Phys. B: Condensed Matter Phys. 14 (2000) 295–300.
[5] A.Y. Liu, M.L. Cohen, Science 245 (1989) 841.
[6] C-Z. Wang, E-G. Wang, Q. Dai, J. Appl. Phys. 83 (1997) 1975.
[7] L.C. Chen, C.K. Chen, S.L. Wei et al., Appl. Phys. Lett. 72 (1998) 2463.
[8] A. Bendeddouche, R. Berjoan, E. Beche, R. Hillel, Surf. Coat. Technol. 111 (1999) 184.
[9] D.Y. Lin, C.F. Li, Y.S. Huang et al., Phys. Rev. B15 (1997) 6498.
[10] A. Badzian, T. Badzian, W.D. Drawl, R. Roy, Diam. Relat. Mater. 7 (1996) 1519.
[11] L.C. Chen, D.M. Bhusari, C.Y. Yang et al., Thin Solid Films 303 (1997) 66.
[12] D.M. Bhusari, C.K. Chen, K.H. Chen et al., J. Mater. Res. 12 (1997) 322.
[13] L.C. Chen, C.Y. Yang, D.M. Bhusari et al., Diam. Relat. Mater. 5 (1996) 514.
[14] L.C. Chen, H.Y. Lin, C.S. Wong et al., Diam. Relat. Mater. 8 (1999) 618.
[15] Z. He, G. Carter, J.S. Colligon, Thin Solid Films 283 (1996) 90.
[16] R. Machorro, E.C. Samano, G. Soto, L. Cota, Appl. Surf. Sci. 127-129 (1998) 564.
[17] W.F.A. Besling, A. Goossens, B. Meester, J. Schoonman, J. Appl. Phys. 83 (1998) 544.
[18] D.J. Johnson, Y. Chen, Y. He, R.H. Prince, Diam. Relat. Mater. 6 (1997) 1799.
[19] Z. Gong, E.G. Wang, G.C. Xu, Y. Chen, Thin Solid Films 348 (1999) 114.